Available online at www.sciencedirect.com
SCIENCE DIRECT
Polymer 46 (2005) 6075–6089
polymer
www.elsevier.com/locate/polymer

Glass transition and free volume in the mobile (MAF) and rigid (RAF) amorphous fractions of semicrystalline PTFE: a positron lifetime and PVT study

G. Dlubek[a,*], A. Sen Gupta[b,d], J. Pionteck[c], R. Häßler[c], R. Krause-Rehberg[b], H. Kaspar[e], K.H. Lochhaas[e]

[a]*ITA Institut für innovative Technologien GmbH, Köthen, Außenstelle Halle, Wiesenring 4, D-06120 Lieskau (bei Halle/S), Germany*
[b]*Martin-Luther-Universität Halle-Wittenberg, Fachbereich Physik, D-06099 Halle/S, Germany*
[c]*Leibniz-Institut für Polymerforschung Dresden e.V, Hohe Strasse 6, D-01069 Dresden, Germany*
[d]*Department of Physics, Visva-Bharati, Central University, Santiniketan 731235, West Bengal, India*
[e]*Dyneon GmbH and Co. KG, Werk Gendorf, D-84504 Burgkirchen, Germany*

Received 20 January 2005; received in revised form 18 April 2005; accepted 18 April 2005
Available online 16 June 2005

Abstract

The structure of the free volume and its temperature dependence in poly(tetrafluoroethylene) (PTFE) and of its copolymer with perfluoro(propyl vinyl ether) (PFA) was studied by pressure–volume–temperature (PVT) experiments ($T=27$–380 °C, $P=0.1$–200 MPa) and positron annihilation lifetime spectroscopy (PALS, $T=-173$–250 °C, $P=10^{-5}$ Pa). From the analysis of these experiments we conclude on the volumetric properties of the mobile (MAF) and rigid amorphous fractions (RAF) in these semicrystalline polymers. The specific volumes of the MAF and RAF, V_{MAF} and V_{RAF}, were estimated assuming that V_{MAF} agrees with the specific volume of the melt extrapolated down to lower temperatures using the Simha–Somcynsky equation of state (S–S eos). V_{RAF} was then estimated from the specific volume of the entire amorphous phase, V_a, and the known V_{MAF}. The specific free volume $V_f=V_a-V_{occ}$ was also estimated from V_a using the S–S eos hole fraction h, $V_{occ}=(1-h)V_a$. From the analysis of PALS data with the routine LT9.0 the mean volume, $\langle v_h\rangle$, and the width, σ_h, of the local free volume size distribution (holes of subnanometre size) were obtained. A comparison of $\langle v_h\rangle$ with V_f delivered the hole density N'_h. The volume parameters show that the RAF which is formed during crystallisation from the melt has a distinctly smaller specific free and total volume than the MAF. During cooling the contraction of the RAF slows down and finally, below room temperature, the RAF possesses a larger free volume than the MAF shows. Obviously, the restriction of the segmental mobility in the RAF by the crystals limits at high temperatures the free volume expansion and at low temperatures dense packing of the polymer chains. These conclusions from the analysis of the specific volume are confirmed by PALS experiments.

Keywords: Free volume; Rigid amorphous fraction; Positron lifetime

1. Introduction

The structure of semicrystalline polymers is still under discussion [1–7]. In the last years it has become clear that a simple two phase model—crystallites embedded in amorphous surroundings—is not sufficient to understand the properties of theses materials. Consensus seems now to be reached that at least three different regions must be considered. The non-crystalline phase must be subdivided into the non-crystalline amorphous and the crystalline-amorphous interfacial portions. The cause for the intermediate interfacial region is the continuation across the phase boundaries of the molecules which are much longer than the phase dimensions. This region is amorphous but has a constrained molecular mobility and is usually described as rigid-amorphous fraction (RAF) [1]. The non-crystalline amorphous region is expected to exhibit properties like the completely amorphous bulk polymers and may be termed as mobile amorphous fraction (MAF). Mechanical and

* Corresponding author. Tel.: +49 345 5512902; fax: +49 40 3603241463.
E-mail address: gdlubek@aol.com (G. Dlubek).

0032-3861/$ - see front matter © 2005 Elsevier Ltd. All rights reserved.
doi:10.1016/j.polymer.2005.04.090

dielectric spectroscopy, nuclear magnetic resonance, Raman spectroscopy, and temperature-modulated calorimetry are employed to investigate semicrystalline polymers [1–7]. However, many questions with respect to the structure and dynamic properties of the RAF remain. One question is, for example, whether the RAF undergoes its own glass transition or vitrifies during crystallisation [5–7].

The purpose of our paper is to contribute to the understanding of these problems. To this aim, we have investigated the volumetric properties on a molecular scale and combined these experiments with macroscopic volume measurements. The free volume of a polymer, particularly the size of local free volumes, is an important parameter, being closely related to the molecular mobility. We will attempt to distinguish the volumetric properties of both amorphous portions, the MAF and the RAF, and to conclude on their temperature dependency and glass transition.

We employed positron annihilation lifetime spectroscopy (PALS) in this study, a method which has developed during the past decade to be an important tool for studying the local free volume of polymers [8–13]. In molecular solids and liquids, a fraction of the positrons injected from a radioactive source forms positroniums [12,13] and these can annihilate from the *para* (*p*-Ps, singlet spin state), or the *ortho* state (*o*-Ps, triplet spin state) with a relative formation probability of 1:3. Three decay components appear in the positron lifetime spectrum of amorphous polymers and these are attributed to the annihilation of *p*-Ps, free (not Ps) positrons, e^+, and *o*-Ps.

In amorphous polymers Ps is formed in subnanometre size holes of the excess free volume (Anderson localisation [14]) When localised at a hole the Ps moves in internal regions of the hole and collides frequently with the molecules of the hole walls. During a collision *o*-Ps may annihilated with an electron other than its bound partner and with opposite spin with the consequence that the (mean) *o*-Ps lifetime decreases from its value in a vacuum, 142 ns (self annihilation), to the low ns-range (1–6 ns, pick-off annihilation [12,13]). The smaller the hole is, the higher is the frequency of collisions, and the shorter the *o*-Ps life. Assuming the shape of the holes (usually spheres) the hole size can be calculated from the *o*-Ps lifetime employing a semi-empirical model [6–10].

In some semicrystalline polymers an extra, intermediate ($\sim$1 ns), *o*-Ps lifetime appears. This lifetime is attributed to *o*-Ps formed in crystals [15–19] and is expected to mirror the lattice plane spacing (interstitial free volume). The lifetime of *o*-Ps annihilation from holes in the amorphous phase can be separated from this lifetime in those cases where both lifetimes are not too similar. In this way the microstructure of the amorphous phase in semicrystalline polymers which contains both the MAF and RAF can be studied. First experiments to investigate these fraction employing PALS can be found in the literature [20–22].

For studying the temperature dependence of the macroscopic volume we performed PVT experiments [23]. We used the Simha–Somcynsky equation of state (S–S eos [24,25]) for an extrapolation of the specific volume from the melt down to lower temperatures, identified this volume with the MAF and used this for an estimation of the RAF volume from the specific volume of the entire amorphous phase. The S–S eos theory also allows the specific occupied and free volume of the equilibrium amorphous phase to be calculated. We will use this information in combination with the results from PALS to conclude on the density of free volume holes. Until now this method has been applied only to completely amorphous polymers [26–32].

As materials of our studies we selected poly(tetrafluoroethylene)s (PTFE) of different crystallinity and a semicrystalline copolymer (PFA) and compared the results with those for a completely amorphous copolymer (PFE) studied previously [32] (for a review of properties of PTFE, PFA, and PFE copolymers see Ref. [33]). One advantage of PTFE is that the intermediate lifetime attributed to *o*-Ps annihilation from crystals can be well separated from that of the amorphous phase which exhibits, due to the stiffness of the tetrafluoroethylene chains, rather large holes. PALS studies of PTFE have been performed already in past [15–18,34,35], very instructive results can be found in the papers of Kindl et al. [15]. The progress in our work is that we used for the analysis of the positron lifetime spectra the new routine LT in its latest version 9.0 [36,37] and correlate the PALS results with those from PVT experiments. The routine LT9.0 allows log normal distributed annihilation rates which lead to a more accurate fitting of the lifetime spectra than when using the conventional discrete term analysis and avoids possible artefacts [38]. Moreover, from the distribution of the *o*-Ps annihilation rate the size distribution of free volume holes and a reasonable value for the mean hole volume can be calculated.

2. Experimental

2.1. Polymers

The samples under investigation were two pure poly(tetrafluoroethylene)s (-[C_2F_4]-) in virgin, as-polymerised (TFv) and sintered, melt crystallised state (TFs), two poly(tetrafluoroethylene)s modified with a small amount, 0.1–2.0 wt%, of perfluoro(propyl vinyl ether) (–[F_2C–$CFOC_3F_7$]–) in virgin (TFMv) and sintered state (TFMs), and a copolymer of tetrafluoroethylene and 2–5 mol% perfluoro(alkoxy vinyl ether) (–[CF_2–$CFOC_xF_{2x+1}$]–, $x=3$–4) in sintered, melt crystallised state (PFAs). Highly crystalline PTFE powder of $\sim$25 μm mean diameter was pressed at room temperature with a pressure of 35 MPa into 2 mm thick plates for making the virgin samples. A second set of samples were sintered at 375 °C under a pressure of 35 MPa for 4 h. Subsequently these samples, plates of 2 mm thickness, were cooled down with a rate of approximately 10 K/min. Table 1 shows the characteristic properties of

Table 1
Sample characterization and volume parameters estimated from PVT data (see text)

Sample	Uncertainty	TFv	TFs	TFMv	TFMs	PFAs	PFE
Polymer		PTFE		PTFE	Modified	PFA	PFE
Treatment		Virgin	Sintered	Virgin	Sintered	Sintered	–
M_w (g/mol)	±10%	10^5	10^5	$\sim 10^5$	$\sim 10^5$	10^4	10^5
DSC, first melting							
ΔH_m (J/g)	±3	64.0	28.4	69.9	26.7	28.3	–
T_m (°C)	±2	344.8	329.3	345.8	326.6	308.0	–
DSC, second melting							
ΔH_m (J/g)	±3	27.9	28.3	32.2	33.3	31.5	–
T_m (°C)	±2	328.6	328.2	324.1	324.0	308.3	–
DSC, cooling, crystallization							
ΔH_c (J/g)	±3	27.9	26.6	32.2	31.1	31.4	–
T_c (°C)	±2	314.2	314.5	308.1	306.2	280.9	–
Density at 27 °C							
ρ (g/cm^3)	±0.0007	2.2693	2.1478	2.2645	2.1487	2.1286	2.0786
V (27 °C) (cm^3/g)	±0.0002		0.4656		0.4654	0.4698	0.4811
T_{me} (°C)	±5	354	336	352	337	325	–
T_{co} (°C)	±5	333	335	330	337	320	–
Crystallinity X_c (%)							
From ΔH_m[a]	±5	78	35	85	33	34	0
From density ρ	±5	85	39	86	39	31	0

[a] First melting.

these samples. For comparison we include in our discussion the results for a completely amorphous copolymer of tetrafluoroethylene (45–85 mol%) and perfluoro(methyl vinyl ether) (–[F_2C–$CF(OCF_3)$]–, 15–55 mol%) denoted as PFE. More details about this material can be found in our previous paper on fluorine elastomers [32]. All of the samples were kindly supplied by Dyneon GmbH and Co. KG, Werk Gendorf, Burgkirchen, Germany. (The exact composition of all samples is known to the authors.)

2.2. Differential scanning calorimetry

Differential scanning calorimetry was performed with a DSC-7 (Perkin-Elmer), PYRIS-software, Version 4.01, in a temperature range between −60 and 360 °C applying heating and cooling rates of 20 K/min. The heating and cooling cycle was: first heat, first cool, second heat. DSC scans are shown in Fig. 1. For clarity we have shown only the thermograms measured during the first heat, and in a restricted temperature range. Two, in case of PFAs one, first order phase transitions in the temperature range between 0 and 35 °C and the melting peak at 300–350 °C can be observed. Not any indications of the glass transition were found at measurements up to minus 170 °C using a DSC 204 (Netzsch).

The crystallinity is estimated from $X_c = \Delta H_m/\Delta H_m^0$ where ΔH_m is the heat of fusion. For 100% crystallinity a heat of fusion of $\Delta H_m^0 = 82$ J/g has been assumed [39–42]. This value has been used also for PFAs assuming that the crystal in this copolymer is made from pure PTFE [41]. The values ΔH_m and X_c are shown in Table 1 together with other parameters estimated from DSC and PVT experiments. T_m and T_c are the midpoint melting and crystallisation temperatures. The melting temperature analysed from the second heating run of the TF samples agrees with the data from the literature, $T_m = 328.5$ °C [40], T_m of TFM is slightly smaller, 324.1 °C. The copolymer PFAs melts at lower temperatures than PTFE, $T_m = 308.3$ °C. The first melting of both virgin samples, TFv and TFMv, shows overheating, while all samples show undercooling before crystallisation at T_c during the cooling runs (Table 1).

The integral enthalpy of the two first-order transitions around room temperature was estimated to lie between 5.9 and 9.9 J/g, depending on the crystallinity of the sample. These transitions are attributed to structural transitions known to occur in the crystalline phase of PTFE at 19 and 30 °C [1,40,42].

2.3. Density measurements

The density ρ of the samples at room temperature (27 °C)

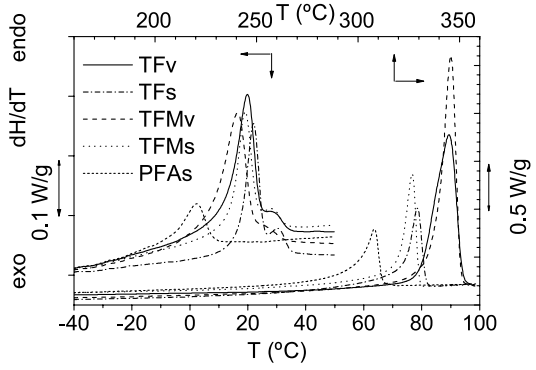

Fig. 1. DSC thermograms (1st heating) of fluoro polymers measured at a heating rate of 20 K/min.

was determined by means of an Ultrapycnometer 1000 (Quantachrome) with an accuracy of 0.03%. From the specific volume $V=1/\rho$ the crystallinity X_c of the samples was estimated via $X_c=(V-V_a)/(V_c-V_a)$ assuming no voids and densities of $\rho_a=2.060$ g/cm^3 for the amorphous and $\rho_c=2.303$ g/cm^3 for the crystalline limit. ρ_c has been estimated from X-ray diffraction experiments [39,40] and ρ_a was obtained from the linear extrapolation of the $V-\Delta H_m$ curve to $\Delta H_m=0$ [40]. As Table 1 shows the crystallinities estimated from DSC and density measurements agree well. The crystallinities of the virgin PTFE samples are estimated to 80–85%, those of the sintered, melt crystallized samples to 30–40%.

2.4. PVT experiments

Isothermal and isobaric PVT measurements were carried out in the temperature range between 22 and 370 °C by means of a fully automated GNOMIX high-pressure dilatometer [20]. The isobaric heating and cooling experiments were performed at a pressure of 10 MPa with a rate of 2 K/min. (Note: when cooling below ca. 100 °C the cooling rate is reduced due to the limited heat exchange). The data of the standard isothermal experiments were collected in steps of 10 K. At every constant temperature the material was pressurised from 10 to 200 MPa. The specific volumes for ambient pressure were obtained by extrapolating the values for 10–30 MPa in steps of 1 MPa according to the Tait equation using the standard GNOMIX PVT software. The accuracy is within 0.002 cm^3/g in the temperature range up to 200 °C, above 200 °C it is 0.004 cm^3/g.

2.5. Thermomechanical measurements

The thermomechanical analysis was performed by a thermomechanical analyser Q400 (TA Instruments) in a temperature range from −100 to 180 °C. The heating rate was 3 K/min. The dimension change $\Delta L/L$ (μm/m) and the linear coefficient of thermal expansion (α in μm/m K) were analysed online in dependence on temperature. The accuracy limits of the heat transitions are within ±3 K, the agreement of the expansion coefficient with the results of the PVT analysis in the overlapping temperature range is acceptable (ca. 30 μm/m K).

2.6. Positron lifetime experiments

The PALS measurements were carried out using a fast–fast coincidence system [12,13] with a time resolution of 232 ps (FWHM, ^{22}Na source) and a channel width of 50.0 ps. Two identical samples of 2 mm thickness and 8×8 mm^2 area were sandwiched around a 1×10^6 Bq positron source: ^{22}NaCl, deposited between two 7 μm thick aluminium foils. To prevent sticking of the source to the samples at higher temperatures, each sample was covered with additional foils of 8 μm thick Kapton and 7 μm thick aluminium. The temperature of the samples, placed in a vacuum chamber of a pressure of 10^{-5} Pa, was varied, between −173 °C and at maximum 250 °C, in steps of 15 K, respectively, with an uncertainty of ±1 K. Each lifetime measurement lasted 6 h. The spectra contained $\sim6\times10^6$ coincidence counts sufficiently high to be analysed with LT9.0 in its distribution mode. In addition to the temperature runs, each sample was measured at room temperature in air to collect $\sim30\times10^6$ coincidence counts in a spectrum. Source corrections, 9.6% of 386 ps (Kapton and NaCl) and 13.6% of 165 ps (Al foils), and time resolution were determined by measuring a defect-free p-type silicon reference ($\tau=219$ ps). The resolution function used in the final spectrum analysis was determined as a sum of two Gaussians with FWHMs of 268 and 385 ps and weights of 79.9 and 20.1%, the second Gaussian is shifted by −0.22 channels with respect to the first one.

3. Results and discussion

3.1. Specific volume and S–S eos analysis of PVT data

Figs. 2–4 present selected results of our PVT experiments. Fig. 2 shows the temperature dependence of the specific volume, V, for the semicrystalline samples and for amorphous PFE at ambient pressure derived from the standard isothermal heating experiments. In case of the sintered samples, TFs, TFMs, and PFAs, and of PFE the cooling curves are very similar to the heating curves. For the initially virgin samples TFv and TFMv the cooling curves measured after melting behave close to those of TFs and TFMs (not shown). Fig. 3 shows 10 MPa isobars for TFs, TFMs, and PFA measured during heating and cooling the samples with rates of 2 K/min.

The heating runs show the thermal expansion of the semicrystalline samples, the melting, and the thermal expansion of the melts. Measurements during cooling show crystallisation, and in case of the melt crystallized samples TFs and TFMs at medium and low temperatures

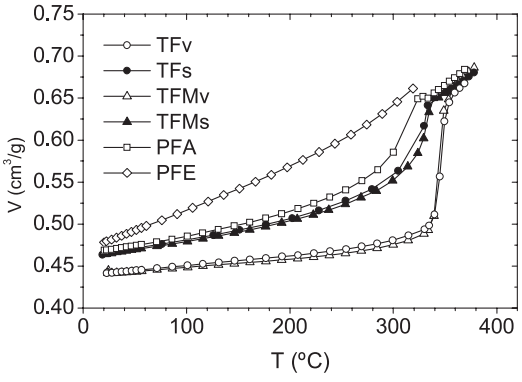

Fig. 2. Specific volume V of fluoro polymers as a function of temperature T at ambient pressure (heating curves).

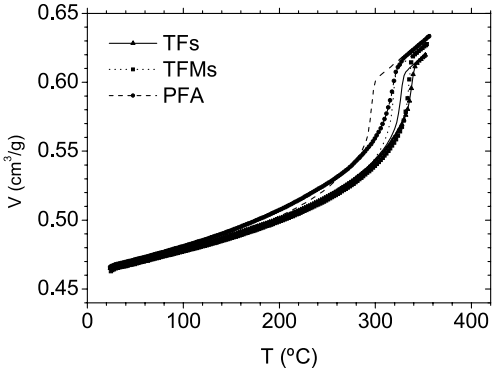

Fig. 3. 10 MPa specific volume isobars V of semicrystalline fluoro polymers, as a function of the temperature T. Lines with symbols: heating curves, lines without symbols: cooling curves (heating and cooling rates of 2 K/min).

almost the same volume as in the heating run. The copolymer PFAs shows a lowering of V (Fig. 3). The melting (end) and crystallisation (onset) temperatures, T_{me} and T_{co}, shown in Table 1, are estimated from the ambient pressure data. T_{me} was defined as temperature at which the last vestige of crystallinity disappeared, and at T_{co} first signs of crystallisation are detectable. These temperatures are therefore higher than the peak temperatures T_m and T_c analysed from DSC. The cooling isobars (Fig. 3) show a distinct undercooling.

Fig. 4 displays, for PFAs as an example, the behaviour of the specific volume V as a function of temperature T and as selection of isobars (in MPa) determined from the isothermal measurements (standard PVT experiments [23]). In the melt, at $T=360$ °C and $P=0.1$ MPa, the isobaric coefficient of thermal expansion has a value of $\alpha_m=(1/V)(dV/dT)_P=1.4(\pm0.05)\times10^{-3}\,K^{-1}$, the isothermal compressibility $\kappa=-(1/V)(dV/dP)_T$ $(P\to0)$ amounts to $\kappa=3.7(\pm0.1)\times10^{-3}\,MPa^{-1}$. The pressure dependence of T_{me} was estimated to $dT_{me}/dP=0.38$ K/MPa for $P<50$ MPa.

The samples TFM consist of almost pure PTFE and show a high Ps yield. We focus therefore in the following parts

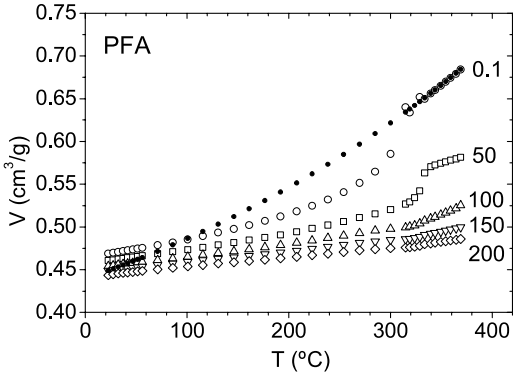

Fig. 4. Specific volume V of semicrystalline PFAs as a function of temperature T and as selection of isobars (in MPa) determined from standard isothermal measurements. Open symbols: experimental data, dots: S–S eos fit (Eq. (2)) to the 0.1 MPa isobar.

our discussion to the ambient pressure data of this material and compare PVT with PALS experiments. Fig. 5 shows the temperature dependence of the specific volume, V, for TFMv and TFMs from heating experiments. Together with these data we have shown the specific volume of PTFE crystals, V_c, as analysed from the wide angle X-ray scattering (WAXS) by Starkweather et al. [39,41]. The thermal expansion of crystals (hexagonal phase I) is almost linear in the temperature range between 35 and 150 °C with a coefficient of $\alpha_c=0.255\times10^{-3}\,K^{-1}$. Above 150 °C, α_c shows an increase with the temperatures and reaches a value of $\alpha_c=0.99\times10^{-3}\,K^{-1}$ at 320 °C. For comparison, the melt shows $\alpha_m=1.38(\pm0.05)\times10^{-3}\,K^{-1}$. The specific volumes show that the virgin polymer is almost crystalline, while the sintered and melt crystallized sample has a distinctly lower crystallinity.

The temperature dependent specific volume of the (entire) amorphous phase in a semicrystalline polymer, $V_a(T)$, can be calculated from the experimental, $V(T)$, and crystalline, $V_c(T)$, specific volume using

$$V_a(T)=\frac{[V(T)-X_cV_c(T)]}{(1-X_c)} \quad (1)$$

where X_c is the mass crystallinity. We assume that X_c is constant up to a temperature of 250 °C and use the value estimated for TFMs from our density measurements at room temperature, $X_c=39\%$. The results of the calculations are shown in Fig. 5.

In order to obtain information on the free volume we analysed the specific volume data employing the S–S eos theory [24,25]. This theory describes the structure of a liquid by a cell or lattice model which allows an occupied lattice-site fraction $y=y(V,T)$ of less then one. Here V is the specific volume of the melt and T is the absolute

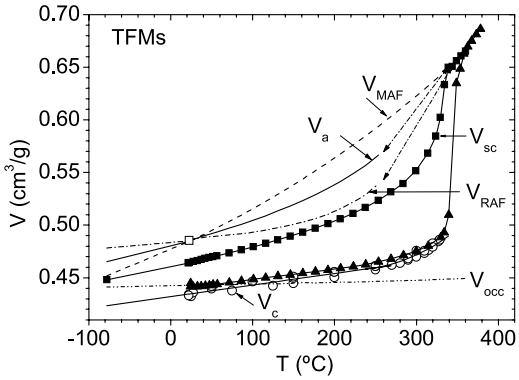

Fig. 5. The specific volume of the sintered, melt crystallized TFMs, V_{sc} (filled squares), the (entire) amorphous phase of TFMs, V_a (solid line, open square: taken from Ref. [40] for amorphous PTFE), and the crystalline phase, V_c (open circles). V_{MAF} (dashed line) and V_{occ} (dash-dot-dotted line) are the specific volume of the mobile-amorphous fraction (MAF) and the specific occupied volume both analysed from the S–S eos, while V_{RAF} (dash-dotted line) denotes the specific volume of the rigid-amorphous fraction (RAF). For comparison the specific volume of the virgin, as polymerized TFMv (filled triangles) is shown.

temperature. The fraction of unoccupied lattice-sites (holes which form the excess free volume) denoted in this theory by h, is given by $h(V, T)=1-y$. The Simha–Somcynsky equation-of state follows from the pressure equation $P=-(\partial F/\partial V)_T$, where $F=F(V, T, y)$ is the configurational (Helmholtz) free energy F of the liquid. It was shown that the specific volume V of the liquid polymer can be expressed by an universal interpolation formula which has in the temperature range $\tilde{T}=0.016$–0.071 and for zero pressure the form [24,25]

$$\ln \tilde{V} = a_0 + a_1 \tilde{T}^{3/2} \tag{2}$$

where the most recent determination by Utracki and Simha [25] delivered $a_0=-0.10346$ and $a_1=23.854$. $\tilde{V}$ and $\tilde{T}$ are reduced variables, $\tilde{V}=V/V^*$, $\tilde{T}=T/T^*$, where V^*, and T^* are characteristic scaling parameters.

Fitting Eq. (2) to the volume data of the melt in the temperature range $T=340$–370 °C delivered for TFMs the parameters $V^*=0.448(\pm0.008)$ cm^3/g and $T^*=8350$ (±100) K which are in close agreement with those published by Rodgers [43] for PTFE, $V^*=0.4339$ cm^3/g and $T^*=8126$ K. For PFAs we obtain $V^*=0.411$ (±0.008) cm^3/g and $T^*=7375(\pm100)$ K (Fig. 4). However, for the completely amorphous PFE we had observed previously that the specific volume increases at temperatures above 200 °C stronger than predicted from the fits of Eq. (2) to experiments below this temperature. This has the consequence that the extrapolation of the fits to the data for higher temperatures to temperatures below 200 °C gives too small volumes compared with the experiment. We expect that this may be also the case for our polymers (compare Fig. 4). To avoid this problem we included in our fits the well accepted completely amorphous volume of PTFE at room temperature, $V=1/2.06=0.4854$ cm^3/g [40]. We assume that this volume can be identified with the equilibrium amorphous volume. The fit of Eq. (2) to the data of the melt and this data point (open square in Fig. 5) delivered for TFMs the parameters $V^*=0.4635(\pm0.003)$ cm^3/g and $T^*=8767(\pm50)$ K. With these scaling parameters the hypothetical equilibrium volume is calculated for a larger temperature range using Eq. (2). We assume that this volume is identical to the volume of the mobile amorphous fraction in the semicrystalline polymers and denote it by V_{MAF}. All volumes displayed in Fig. 5 were extrapolated to $T=-80$ °C$\approx T_g$ (see below).

The fraction of unoccupied lattice sites, h, of a liquid polymer at zero pressure can be calculated from the universal algebraic expression

$$h(T) = a_0 + a_1 \tilde{T} + a_2 \tilde{T}^2 \tag{3}$$

derived in the paper of Utracki and Simha [25] where $a_0=-0.09211$, $a_1=4.892$, and $a_2=12.56$. We found that this approximation gives almost the same h-values as the numerical solution of the explicit pressure equation for our polymers (Ref. [24]). With the knowledge of h, the specific occupied and the (hole or excess) free volume can be calculated from $V_{occ}=yV=(1-h)V$ and $V_f=V-V_{occ}=hV$ where here $V=V(T/T^*, V^*)=V_{MAF}$ is the calculated equilibrium amorphous volume.

The behaviour of the calculated occupied volume V_{occ} in the range between T_g and the melt is also shown in Fig. 5. Its value at room temperature, $V_{occ}=0.443$ cm^3/g, is slightly higher than the crystalline volume known from WAXS experiments (phase I, $T>30$ °C), $V_c=1/2.313=0.434$ cm^3/g [39–41]. The relations $V_{occ}\approx V_c$ and $V_{occ}/V_W=1.50$, ($T\geq T_g$,$V_W=0.296$ cm^3/g—van der Waals volume of PTFE) seem to be generally valid for polymers [27–32]. The occupied volume contains, like the crystalline, a free volume inherent to each lattice cell (interstitial free volume $V_{fi}=(1.5-1)V_W=0.5\ V_W$ [24]). The total volume of an amorphous polymer is composed of the occupied, V_{occ}, and the hole or excess free volume, V_f, $V=V_{occ}+V_f=V_W+V_{fi}+V_f$. This excess free volume is calculated in the S–S theory as the sum of volume of all empty lattice cells, $V_f=hV$. In approximation V_f can be estimated from $V_f=V-V_{occ}=V-1.50\ V_W=0.14\ V_W$ ($V=V_{MAF}=0.4854$ cm^3/g$=1.64V_W$, at $T=27$ °C). A certain amount of this excess free volume is necessary to allow segmental motions [44,45]. The excess free volume is therefore closely related to the glass transition. The expansion of the polymer above T_g occurs in the S–S theory mainly due to the creation of new empty lattice cells. As we have shown recently, the fraction of the empty cells, h, follows for amorphous polymers an Arrhenius law with a formation enthalpy being approximately half of the cohesive energy [30,32].

The coefficient of thermal expansion of the occupied volume amounts to $\alpha_{occ}=0.52\times10^{-4}$ K^{-1}. This value is distinctly smaller than that of the crystalline volume, $\alpha_c=2.55\times10^{-4}$ K^{-1} [39–41] (all at room temperature). Such small values of α_{occ} we observed also previously for the fluoroelastomer PFE ($V_{occ}=0.431$ cm^3/g, $V_{occ}/V_W=1.44$, $\alpha_{occ}=0.38\times10^{-4}$ K^{-1}, all for $T=300$ K ($>T_g$), see Table 1 in Ref. [32]) and for polystyrene ($V_{occ}=0.895$ cm^3/g, $V_{occ}/V_W=1.49$, $\alpha_{occ}=0.22\times10^{-4}$ K^{-1}, $T>T_g$, $T\rightarrow T_g=100$ °C [30]), for example. We notice for TFMs the relation $V^*/V_W=1.51$ (PFE: 1.59, PS: 1.55) which is close to that found by other groups for a larger variety of polymers, ~1.45 [46] and 1.57–1.60 [27]. Moreover, we found $K(T/T^*)=V_{occ}/V^*=0.969$ (PFE: 0.956, PS: 0.955). In the literature an approximation for h is frequently calculated from $h=1-K/(V/V^*)$ assuming a constant $K=0.96$ [24].

The specific volume of the rigid amorphous fraction, V_{RAF}, may now be estimated from

$$V_{RAF} = \frac{[V_a - RV_{MAF}]}{(1-R)} \tag{4}$$

where R is the mass fraction of the MAF in the entire amorphous volume V_a and $V_{MAF}=V$ is given by Eq. (2). The relations $X_c+X_a=X_c+X_{MAF}+X_{RAF}=1$, $X_{MAF}=X_aR$,

and $X_{RAF}=(1-R)X_a$ are valid. Here X_a, X_{MAF}, and X_{RAF} are the mass fraction of the entire amorphous phase, of the MAF, and RAF, respectively. Since R is not known we assumed tentatively a value of $R=0.5$ (see our estimation in one of the next chapters) to be representative for the sintered and melt crystallised sample. Due to this assumption, V_{RAF} proceeds at higher temperatures below V_a as much as V_{MAF} is above (Fig. 5).

At room temperature both curves intersect because we have used the value 0.4854 cm^3/g for calculating both V_{MAF} and V_a. The assumption of a crystallinity of $X_c=33\%$ as estimated from DSC experiments gives a smaller value of V_a but does not change the whole picture. The behaviour of V_{RAF} may be understood in the following way. When coming from the melt and decreasing the temperature crystallisation starts at T_{co}. A fraction of the amorphous phase, the RAF, becomes restricted in its segmental mobility due to the incorporation of polymer chains into the crystals. Our results show that this process is associated with denser molecular packing and a distinct loss of free volume compared with the unconstrained amorphous phase. Owing to its high mobility the MAF shows stronger thermal volume fluctuations near T_c which are realised by co-operative motions leading to large local free volumes (transient holes) and a large specific free volume (Fig. 6).

At medium temperatures the contraction of the RAF slows down and finally, below room temperature, the RAF shows a larger specific volume than the MAF has (Fig. 5). This behaviour mirrors the restriction in mobility of the RAF by the crystals which now prevents dense packing of the polymer chains. In the MAF, however, packing becoming denser with decreasing temperatures until T_g is reached. Although the accuracy of our volume estimations is not very high and the estimations are based on several assumptions, we think that this picture describes the behaviour of both parts of the amorphous phase in semicrystalline PTFE correctly. We have observed this behaviour for all of the polymers under study in this work.

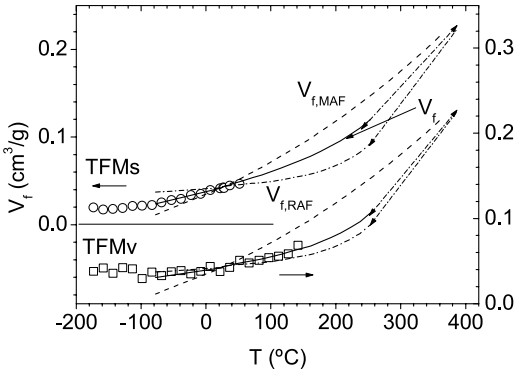

Fig. 6. The specific free volume of the MAF ($V_{f,MAF}$, dashed line) and RAF ($V_{f,RAF}$, dash-dotted line) and of the entire amorphous phase (V_f, solid line) for the sintered, TFMs ($X_c=39\%$), and virgin, TFMv ($X_c=86\%$), samples. The circles and squares are estimates from PALS for TFMs and TFMv (see text).

An independent confirmation will be given later by our PALS studies. Similar specific volume relations of RAF and MAF as found in our work were determined to be valid for poly(ethylene terephthalate) at room temperature ($T_g=80$ °C) [21,22].

For the calculation of the excess free volume in the entire amorphous phase, V_f, we assume that the occupied volume is the same in both regions, the RAF and MAF. Then this free volume can be calculated from

$$V_f = V_a - V_{occ} \quad (5)$$

where $V_{occ}=V_{occ,MAF}$. V_f represents the average of the specific free volume of the RAF and MAF phases, the weighting factors are the mass fractions of both portions of the amorphous phase, $(1-R)$ and R. The specific free volume of the RAF is $V_{f,RAF}=V_{RAF}-V_{occ,RAF}$, that of MAF $V_{f,MAF}=V_{MAF}-V_{occ,MAF}$, where we assume $V_{occ,RAF}=V_{occ,MAF}$.

Fig. 6 shows the result of these calculations where, again, $R=0.5$ (solid line) has been assumed for TFMs. The specific free volumes behave similarly to the total specific volume since the same occupied volume is assumed in both amorphous phases. The extrapolated specific free volume of the MAF at $T=-80\,°C\approx T_g$, $V_f=0.01131\ cm^3/g$, corresponds to a fractional free volume of $f_g=h_g=V_f/V_{MAF}=0.01131/0.44116=0.026$. This value agrees with an estimation by Williams, Landel, and Ferry [47] from viscosity data of a variety of polymers, $f_g=0.025$ (WLF equation with $B=1$), which was believed for a long period to be of general validity. Other authors [46] showed that f_g increases from ~ 0.02 for polymers with $T_g=200$ K to $f_g\approx 0.08$ for polymers with $T_g=400$ K, a result which was confirmed recently [27]. From this result it was concluded that the glass transition is not an iso-free volume transition but rather determined by the structural relaxation time. We remark that the amorphous copolymer PFE has an exceptionally high value of $f_g=h_g=0.084$ although T_g is rather low, $T_g=-8$ °C (from PALS) [32]. Obviously, this rule may be broken when the structure and mobility of the polymer favours this.

For the highly crystalline, virgin sample TFMv, the RAF should occupy a distinctly larger fraction of the entire amorphous phase than for TFMs. The dashed-dotted curve in Fig. 6 showing the behaviour of $V_{f,RAF}$, was calculated with the tentative assumption of $R=0.25$. A further discussion of these curves, together with the results from PALS (circles and squares in Fig. 6) will be given later.

3.2. The analysis of positron lifetime spectra

In previous papers [18,48] some of us have investigated in detail how many lifetime components appear in PTFE and what their nature is. Based on these results and in agreement with conclusion of other groups [15,35] we decompose the lifetime spectra of PTFE into four

components, $s(t)=\sum(I_i/\tau_i)\exp(-t/\tau_i)$, $\sum I_i=1$, $i=1\ldots4$, attributed to annihilation of *p*-Ps, $\tau_1\approx0.125$ ps, free (e^+, not Ps) positrons, $\tau_2=300$–350 ps, *o*-Ps in crystals, $\tau_3\approx1$ ns, and *o*-Ps in amorphous regions, $\tau_4=2$–6 ns. Usually, the components of the lifetime spectrum are assumed to be discrete exponentials, $\exp(-t/\tau_i)$, with a time constant τ_i or a decay rate $\lambda_i=1/\tau_i$, and a relative intensity of I_i.

Since in the amorphous phase *o*-Ps annihilates from holes of the free volume which have a size and shape distribution the *o*-Ps lifetime [49,50], and probably also the e^+ lifetime [32], will show a distribution. In previous papers some of us have shown that the discrete term analysis of lifetime spectra of both amorphous [51] and semicrystalline [52] polymers may lead to incorrect lifetimes τ_i and intensities I_i when the dispersion in lifetimes is not taken into account. The routines CONTIN (inverse Laplace transformation [35,53]) and MELT (maximum entropy method [54]) allow the user to calculate the lifetime distributions numerically (without assuming an analytical shape of the distribution), however, due to the high degree of freedom in this kind of analysis the results show a high statistical scatter and are also not free of artefacts [38,51,52]. We used the routine MELT for analysing the 30×10^6 count spectra and could confirm that in each of our semicrystalline samples four lifetime components appear, whereas for the amorphous fluoroelastomer PFE only three were found.

As mentioned, the new routine LT9.0 assumes that for some, or all of the annihilation channels, the annihilation rates λ_i, $\lambda_i=1/\tau_i$, follow a log-normal function [36,37]. The non-linear least-squares fit of these functions, convoluted with the resolution function, to the spectra provides the mean lifetime τ_i and the corresponding intensity I_i of the annihilation channel *i* as well as the corresponding lifetime dispersion (standard deviation σ_i of the lifetime τ_i). The assumption of the functional shape of the lifetime distribution which comes from the experiences with the CONTIN routine reduces strongly the degree of freedom in the analysis and leads to sufficient correct and precise results [38].

The number of fitting parameters in unconstrained four-components LT fits is 13: four τ_is, four σ_is, three I_is, the time zero t_0 and the background B. This high number causes a large scatter in the fit parameters where the allowance of the dispersion in the lifetimes is one of the largest sources of these errors. Therefore, we tested first different modes of analysing the lifetime spectra and the consequences on the obtained fitting parameters. Unconstrained fits showed that $\tau_1=100$–140 ps, $I_1/(I_3+I_4)\approx1/3$, and $\sigma_1=\sigma_3\approx0$. Consequently, we constrained in the final fits the *p*-Ps lifetime to its value in vacuum, $\tau_1=125$ ps (i.e. neglectable pick-off annihilation; relaxation parameter of $\eta=1$ in agreement with Refs. [32,55]) and its intensity to the theoretical ratio of the *p*-Ps/*o*-Ps formation probability, $I_1/(I_3+I_4)=1/3$ [10,11], and moreover, $\sigma_1=\sigma_3=0$. The background B was determined from fitting the spectra at very high lifetimes of 38–40 ns. Free floating fit parameters are now τ_2, τ_3, τ_4, σ_2, σ_4, I_3, I_4, and t_0. All of these parameters, except t_0, are affected by material properties. The reduced chi-squares of the fits, χ^2/df, varied for this mode of analysis between 0.98 (100 K) and 1.12 (473 K). When assuming only discrete components, as usually done in past, values of $\chi^2/df=1.2$–1.5 were obtained. The constrained fits delivered the same behaviour of lifetime parameters as the unconstrained analysis, but the statistical scatter of the fit parameters is distinctly smaller.

Figs. 7 and 8 show the temperature dependence of *o*-Ps annihilation parameters for TFMv and TFMs, as an example. The larger *o*-Ps lifetime, τ_4, mirrors the mean size of holes (local free volumes) in the amorphous phase. It shows in the sintered sample TFMs a typical glass transition behaviour: a small increase below $T\approx-85$ °C and a distinctly stronger one above. The temperature where the expansivity in τ_4 increases sharply is usually interpreted as glass transition temperature, $T_g=-83(\pm5)$ °C. The virgin polymer TFMv shows a similar behaviour but with smaller changes in τ_4 and a higher T_g of about -30 °C. Below the glass transition, τ_4 is larger in virgin than in the sintered samples, this tendency reverses above T_g. The dispersion σ_4 which indicates the width of the hole size distribution behaves correspondingly to τ_4. Unfortunately, the resolution of the PALS technique is not high enough to distinguish the holes in the RAF from those in the MAF, τ_4 is an integral *o*-Ps lifetime representing the entire amorphous phase.

The lifetime, τ_3, attributed to *o*-Ps annihilation in crystals, is expected to mirror the lattice plane spacing (interstitial free volume) and in that way the crystalline packing density C. τ_3 varies approximately linearly with C. From the study of perfect low molecular crystals [56] the relation $\tau_3=7.92$–$9.616C$ can be derived. For the polymers under investigations the values of τ_3 vary between 1.0 and 1.15 ns corresponding to packing densities C of 0.720–0.704.

The question arises whether the behaviour of τ_3 mirrors the structural phase transitions occurring in PTFE crystals.

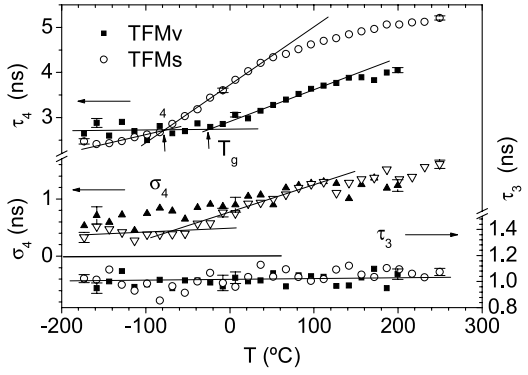

Fig. 7. *ortho*-Ps lifetime from crystalline (τ_3) and amorphous regions (τ_4) and dispersion σ_4 of the *o*-Ps lifetime as a function of the temperature for virgin (v) and sintered, melt-crystallised (s) TFM.

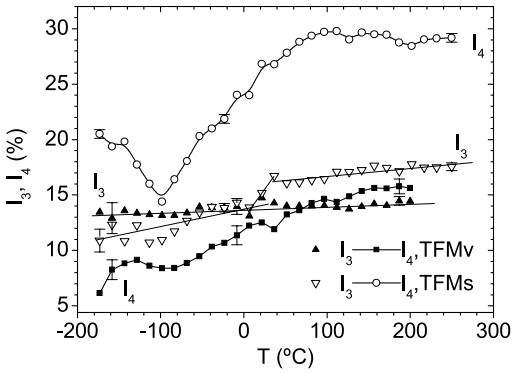

Fig. 8. As in Fig. 7 but intensity of *o*-Ps annihilation from crystalline (I_3) and amorphous regions (I_4).

At low temperatures PTFE crystals exhibit a triclinic structure with molecular chains possessing a $1\times13/5$ helical twist. At 19 °C the amplitude of the torsional oscillations of the molecule increases strongly and results in a new, trigonal crystal structure that accommodates a $1\times15/7$ helix with increasing disorder along the chain. Above 30 °C, the longitudinal order and, therefore, the three-dimensional character of lattice are completely lost by further conformational disordering of the helix ([1,57,58] and references given therein). The DSC scans in Fig. 1 show these two phase transitions, which appear in the modified samples TFMv and TFMs at slightly lower temperature than in the pure PTFE. For the copolymer PFAs only one peak with a maximum at −3 °C appears. Fig. 9 shows the relative change of the linear sample dimension $\Delta L/L$ as a function of temperature. Obviously, only the lower transition causes a step-like increase in the sample volume by $3\times(0.36–0.43)\% = 1.08–1.29\%$. This corresponds to an expected increase in τ_3 of ∼0.10 ns.

In Fig. 10 we have shown τ_3 and I_3 for the pure, sintered and melt crystallised, sample TFs. Like for our other samples (compare Fig. 7), no clear increase in τ_3 can be observed. Unfortunately, the allowance of distributed lifetimes in the spectrum analysis increases strongly the statistical errors of the lifetime parameters. I_3, however, shows a clear, step-like increase by 1.5% near the solid-solid phase transition at −19 °C. Due to energetic reasons an increased Ps formation is expected when more free volume is available [59]. Kindl et al. [15] have observed at −19 °C a distinct increase in I_3 and a smaller one in τ_3 when analysing the positron lifetime spectra assuming four discrete lifetimes. Therefore, we have applied this kind of analysis to our spectra, the results are shown in Fig. 10. Now the step in I_3 occurs more pronounced and τ_3 seems to respond to the crystalline transitions. We believe, however, that this increase in τ_3 is probably an artefact of the spectrum analysis. As discussed previously by some of us in detail [52], the assumption of discrete lifetimes leads to a coupling of the analysed τ_3 to the values of τ_4 and I_4. Thus, the observed increases in τ_3 could be the result of the increase in τ_4 and I_4 above the glass transition at − 83 °C, and in I_3 at 20 °C. Further research may resolve this question.

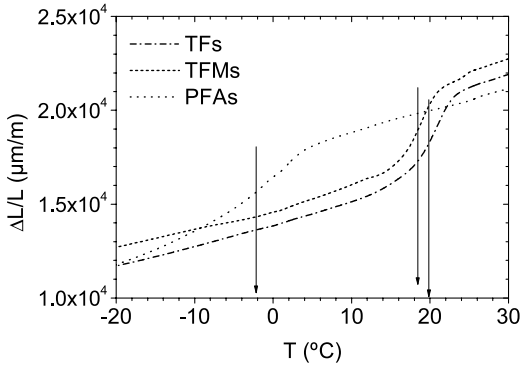

Fig. 9. Relative change, dL/L, of the sample dimension of TFs, TFMs, and PFAs as function of the temperature T.

The *o*-Ps intensities I_3 and I_4 (Fig. 8) mirror the Ps formation probabilities, P_c and P_a ($I=3P/4$), in the crystalline and the amorphous phase, and the fractions of the crystalline and (entire) amorphous phase, X_c and X_a, $X_c+X_a=1$. In a naive picture one may expect $I_3=(3/4)P_cX_c$ and $I_4=(3/4)P_aX_a$. It is generally expected that, due to the dense packing of the crystalline phase, P_c is distinctly smaller than P_a. From the intensity ratio for TFMv at room temperature, $I_3/I_4=14.0/12.5=1.12$ and $X_c/X_a=86/14=6.14$ (from density) one estimates $P_c/P_a=0.18$. I_4 of the virgin sample is smaller by a factor of ∼2 compared with the sintered sample. A linear increase in I_4 with decreasing X_c is frequently observed in the literature [60]. Surprisingly, I_3 does not show the expected decrease with decreasing crystallinity X_c. Although already observed in past for PTFE [15], syndiotactic polystyrene [61], and poly(ethylene terephthalte) [62], the reasons for a non-linear behaviour of I_3 or I_4 are not exactly known. *o*-Ps formation is a very complex process and a variation of P_c and P_a and an *o*-Ps exchange between the crystalline and amorphous regions

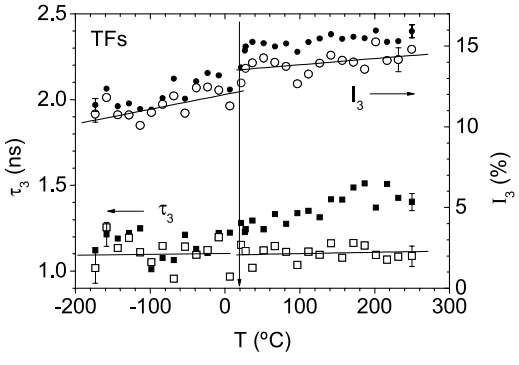

Fig. 10. *ortho*-Ps lifetime τ_3 and intensity I_3 from crystalline regions of TFs as a function of the temperature T. Filled symbols: unconstrained four term analysis assuming discrete lifetimes, open symbols: constrained analysis ($\tau_1=0.125$ ns, $I_1/I_3=1/3$) allowing a dispersion in the lifetimes in the second and fourth component ($\sigma_2>0$, $\sigma_4>0$). The lines are linear fits to the data represented by open symbols in the two temperature ranges below 0 °C and above 35 °C. The arrow shows $T=19$ °C.

may result in non-linear relation between I_3 and X_c, respectively I_4 and X_a. Some authors concluded that *o*-Ps formed in crystallites of syndiotactic polystyrene may diffuse rapidly into the amorphous phase, where localization at free volume holes and annihilation occurs [62]. A similar effect can be expected for the Ps precursor e^+, which has a much larger diffusion length in polymer crystals compared with amorphous polymers [12].

The lifetime τ_2 (not shown) which comes from the positron (e^+, not Ps) annihilation mirrors the integral effect of the empty space in amorphous and crystalline regions. It shows similar behaviour to τ_4. For TFMs τ_2 is almost constant below -80 °C, $\tau_2 = 0.300(\pm 0.003)$ ns. It increases between -100 °C and room temperature rapidly to $\tau_2 = 0.342$ ns followed by a slight increase to $\tau_2 = 0.350$ ns at 250 °C. The dispersion in the positron lifetime, σ_2, shows a behaviour corresponding to τ_2. It increases from $\sigma_2 = 0.03(\pm 0.005)$ ns below -80 °C to $\sigma_2 = 0.07$ ns above room temperature. The lifetime τ_2 of the virgin sample TFMv shows a similar behaviour as for the sintered sample. However, below -100 °C it exhibits a constant value of $\tau_2 = 0.328$ ns which is distinctly larger than for TFMs. Obviously, the as-polymerised, virgin sample exhibits below T_g in the mean a larger local free volume than the melt-crystallised sample. We already observed the same effect in τ_4.

Figs. 11 and 12 show the lifetime, τ_4, and intensity, I_4, of *o*-Ps annihilation in the amorphous phase of the melt-crystallised samples TFs, TFMs, and PFAs, and, for comparison, in the completely amorphous PFE. The glass transition occurs in TFs and TFMs at -80 and -83 °C, in PFAs at -73 °C, and in the elastomer PFE at -8 (± 5) °C. The semicrystalline polymers show at higher temperatures a slowing down of the increase in τ_4, while for the amorphous PFE a complete levelling-off of the increases is observed at a temperature of 120 °C denoted as 'knee' temperature T_k [32].

The *o*-Ps intensity I_4 shows a minimum at -100 °C in the semicrystalline polymers followed by a strong increase above T_g (Fig. 12). This increase is also observed for PFE. At 100 °C all samples show a levelling-off in the increases in I_4. A similar behaviour has been also observed for other polymers, for example for polyethylene (PE) and its copolymers [20]. It was found that the Ps yield in PE increases at temperatures of -200 °C and lowers with increasing duration of positron irradiation. This effect was explained by the accumulation of secondary electrons shallowly trapped by radicals [63,64]. Thermalisation of the positron injected from the source creates excess electrons and free radicals due to the ionisation. Positrons may combine with shallowly trapped electrons to form Ps. A decrease in I_3 above -170 °C was interpreted as a release of weakly bound electrons by the thermal activation of molecules and the recombination of free electrons with reactive species (cations and radicals containing non-saturated bonds). It was also found that irradiation with

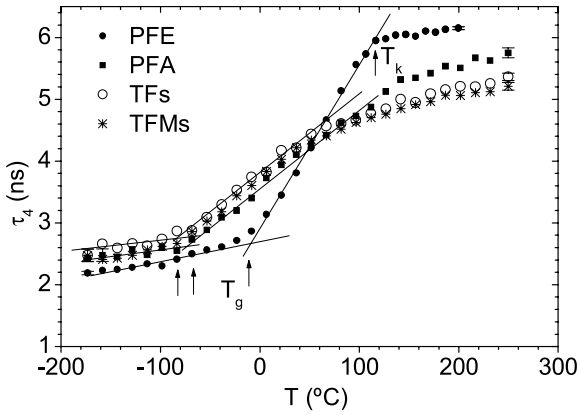

Fig. 11. *ortho*-Ps lifetime from amorphous regions, τ_4, as a function of the temperature for the semicrystalline polymers, TFs, TFMs, and PFAs, and for the amorphous fluoroelastomer PFE.

visible light causes the same effect [63]. Above T_g, the concentration of reactive centres will decrease due to the recombination of mobile ions and radicals. This may lead to the new increase in the *o*-Ps intensity observed for all of our samples (Figs. 8 and 12).

3.3. Hole size distribution and the mean hole size

In the following we focus our discussion on the mean hole size and the hole size distribution calculated from the *o*-Ps lifetime τ_4 and its distribution. Usually the mean radius $r_h(\tau_4)$ of the holes (assumed spherical) is calculated from the (mean) *o*-Ps lifetime $\tau_4 = 1/\lambda_4 = 1/\lambda_{po}$ using the equation

$$\lambda_{po} = 2\ \mathrm{ns}^{-1}\left[1 - \frac{r_h}{r_h + \delta r} + \frac{1}{2\pi}\sin\left(\frac{2\pi r_h}{r_h + \delta r}\right)\right] \qquad (6)$$

where λ_{po} is the annihilation rate of *o*-Ps due to the pick-off process inside the holes. This equation comes from a semi-empirical model [8] which assumes that *o*-Ps is localised in an infinite high potential well with the radius $r_h + \delta r$ where r_h is the hole radius and the empirically determined $\delta r = 1.66$ Å [9,10] describes the penetration of the Ps wave function into the hole walls. The relation $\lambda_{po} = 1/\tau_4$ is based on the assumption that spin conversion and chemical

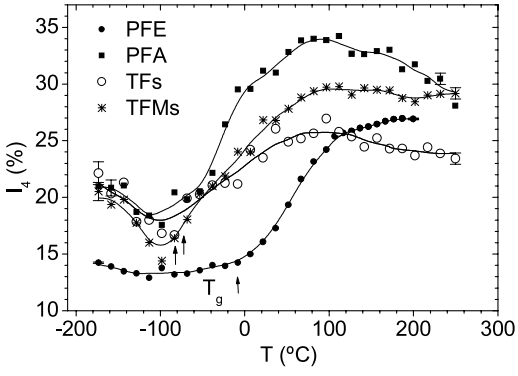

Fig. 12. As in Fig. 11, but the *o*-Ps intensity I_4 (T_g from Fig. 11).

quenching of Ps [12,13] are negligible. The mean hole volume follows then from $v_h(\tau_4)=(4/3)\pi r_h(\tau_4)$.

This usual way of calculating the mean hole volume, however, does not agree with the true mean of the hole size distribution since the relation between τ_4 and the hole volume v_h is not linear. A more reasonable way is to calculate the mean hole volume as mass centre of the hole volume distribution which itself can be calculated from the annihilation rate distribution $\alpha_i(\lambda)$ of the fourth annihilation channel. LT9.0 assumes the quantities $\alpha_i(\lambda)\lambda$ to be log normal functions. The position of the maximum of the distribution for the fourth annihilation channel, λ_{40}, and its the standard deviation $\sigma_4(\lambda)$ are related to the mean *o*-Ps lifetime, τ_4, and its dispersion, σ_4, via $\tau_4=\exp[\sigma_4^2(\lambda)/2]/\lambda_{40}$ and $\sigma_4=\sigma(\tau_4)=\tau_4[\exp(\sigma_4^2(\lambda)-1]^{0.5}$, respectively [36,37]. With Eq. (6) and the known distribution $\alpha_4(\lambda)$ of the *o*-Ps annihilation rates the hole radius probability distribution, $n(r_h)=-\alpha_4(\lambda)\mathrm{d}\lambda_4/\mathrm{d}r_h$, can be calculated from [49,50]

$$n(r_h) = -3.32\left\{\cos\left[\frac{2\pi r_h}{(r_h+\delta r)}\right]-1\right\}\frac{\alpha_4(\lambda)}{(r_h+\delta r)^2} \quad (7)$$

The fraction of the free volume holes with radii between r_h and $r_h+\mathrm{d}r_h$ is $n(r_h)\mathrm{d}r_h$. From Eq. (7) the volume fraction hole size distribution,

$$g(v_h) = \frac{n(r_h)}{4\pi r_h^2} \quad (8)$$

and the number fraction hole size distribution,

$$g_n(v_h) = \frac{g(v_h)}{v_h} \quad (9)$$

can be calculated. $g(v_h)$ gives the volume fraction of free-volume holes with volume between v_h and $v_h+\mathrm{d}v_h$, while $g_n(v_h)$ shows the number fraction of holes with volume between v_h and $v_h+\mathrm{d}v_h$. The normalisation of the distributions is $\int g(v_h)\mathrm{d}v_h=\langle v_h\rangle N_h=f$ where f ($\equiv h$) is the fractional hole free volume, $\langle v_h\rangle$ and N_h are the mean (number averaged) volume and mean number density of holes. The distribution $g_n(v_h)$ may be approximated by a log-normal function, a Γ-function, or more roughly by a Gaussian in agreement with the theoretical considerations of Robertson [65] and Bueche [66]. We have calculated the mean, $\langle v_h\rangle$, and the variance, σ_h^2, of the hole size distribution numerically as first and second moment of the $g_n(v_h)$ distribution.

Figs. 13–15 show the temperature dependence of $\langle v_h\rangle$ and σ_h for free volume holes in the (entire) amorphous phase of the semicrystalline polymers. Results for the amorphous PFE from our previous work [32] are included in Fig. 13. Since both values, τ_4 and σ_4, go in into its calculation, $\langle v_h\rangle$ shows a larger scatter than τ_4. The statistical scatter for the PFE data is smaller than for the semicrystalline polymers since only three lifetime components appear here, $I_3=0$.

The mean hole size in PFAs shows a typical glass transition behaviour as known from amorphous polymers and shown by PFE (Fig. 13). At low temperatures, *o*-Ps is trapped in local free volumes within the glassy matrix and $\langle v_h\rangle$ mirrors the size of static holes. The averaging occurs over the hole size and shape. The slight increase in $\langle v_h\rangle$ with temperature shows the thermal expansion of free volume in the glass due to the anharmonicity of molecular vibrations and local motions in the vicinity of the holes. At a temperature of −85 °C for PFAs and −8 °C for PFE, which, as mentioned, are considered as (volumetric) glass transition temperatures T_g, $\langle v_h\rangle$ shows a distinct increase in its expansivity. The coefficient of thermal expansion of holes changes for PFAs from $\alpha_{hg}=(1/\langle v_{hg}\rangle)\mathrm{d}\langle v_h\rangle/\mathrm{d}T\approx 0.2\times 10^{-3}\,\mathrm{K}^{-1}$ ($T<T_g$) to $\alpha_{hr}=(1/\langle v_{hg}\rangle)\mathrm{d}\langle v_h\rangle/\mathrm{d}T\approx 8.9\times 10^{-3}\,\mathrm{K}^{-1}$ ($T>T_g$) where $\langle v_{hg}\rangle$ is the mean hole volume at T_g (Table 2). This behaviour is due to the rapid increase in the molecular and segmental mobility in frequency and amplitude above T_g. Now $\langle v_h\rangle$ represents an average value of the local free volumes whose size and shape fluctuate in space and time. The increase in $\langle v_h\rangle$ is distinctly steeper for PFE than for PFAs. It mirrors the thermal expansion of the completely mobile amorphous phase in PFE, while for PFAs and all other semicrystalline samples $\langle v_h\rangle$ is an average over the MAF and RAF.

PFE shows at $T_k=110$ °C a levelling-off in the increase in $\langle v_h\rangle$. Different effects such as *o*-Ps detrapping from holes, *o*-Ps bubble formation, the disappearance of the dynamic heterogeneity, or segmental relaxation times in the order of the *o*-Ps lifetime or smaller are discussed as possible reasons for this behaviour [67,68]. For PFAs the increase in $\langle v_h\rangle$ begins to slow down already at about 40 °C. This may be due to the same effects mentioned for PFE. In case of semicrystalline polymers, however, the restriction of the molecular motion and therefore also of the thermal expansion of the RAF by the crystalline phase (and possibly of the MAF by the RAF) may be an additionally probable reason for this behaviour. The width of the hole volume distribution, σ_h, is small and almost constant below T_g. Above that temperature σ_h increases approximately parallel to $\langle v_h\rangle$.

TFMs shows a similar variation in $\langle v_h\rangle$ and σ_h as PFAs

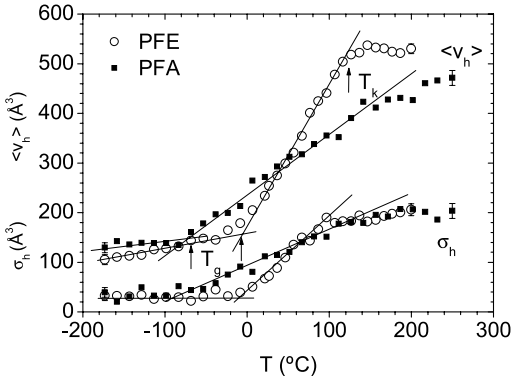

Fig. 13. Mean volume, $\langle v_h\rangle$, and standard deviation, σ_h, of the hole size distribution $g_n(v_h)$ as a function of the temperature T for semicrystalline PFAs and amorphous PFE.

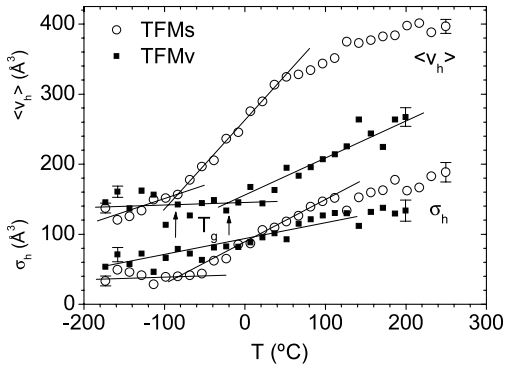

Fig. 14. Mean volume, $\langle v_h \rangle$, and standard deviation, σ_h, of the hole size distribution $g_n(v_h)$ as a function of the temperature T for TFM in virgin (v) and sintered, melt-crystallised state (s).

but exhibits smaller values of these quantities at higher temperatures (Fig. 14). This difference can be attributed to the higher crystallinity of TFMs compared with PFAs. The highly crystalline sample TFMv shows a behaviour which differs from TFMs in several aspects. At low temperatures $\langle v_h \rangle$ and more clearly σ_h are larger than for TFMs. This behaviour delivers evidence that the restriction of the mobility in the RAF by crystals inhibits at low temperatures dense packing of polymer chains. A fraction of holes occurs which are larger than in the MAF. At high temperatures the effect is opposite: the restriction of the mobility in the RAF limits the thermal expansion of the holes and leads to a lower mean hole size than for the sample with lower crystallinity, TFMs. We have already observed this effect in the macroscopic volume (Fig. 5). The pure PTFE samples, TFv and TFs, show a similar behaviour (Fig. 15) as the modified samples, however, due to the lower I_4, with a larger statistical scatter.

It is interesting that the highly crystalline samples TFv and TFMv also show a distinct increase in the hole expansivity though at temperatures of −15 to −20 °C which is higher than the T_gs of the melt crystallized samples by 53–65 °C. If we assume, as in Ref. [20], that an abrupt increase in the slope of the $\langle v_h \rangle$-T curve indicates the glass transition in a mobile amorphous portion, then this behaviour can be considered as evidence that also in our

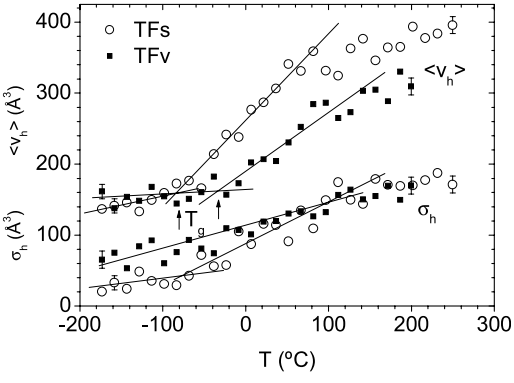

Fig. 15. As in Fig. 14, but for TFv and TFs.

highly crystalline samples a MAF exists. Obviously, its fraction X_{MAF} is smaller and a larger restriction in its mobility by the crystals (and the RAF) occurs than in the MAF of samples with lower crystallinity. Owing to this, higher temperatures are needed to stimulate segmental motions. Recently, it has been observed that the frequency of segmental (α-) relaxation drops down by two orders of magnitude due to the crystallization of poly(dimethylsiloxane) [69]. We remark that in high density polyethylene of 70% crystallinity a glass transition in the mean hole volume has not been seen using PALS [20]. It was concluded from this observation that this polymer contains no MAF but only RAF. In ethylene/1-octene copolymers with crystallinities of 42% and less, however, the glass transition has been observed. The fraction of MAF and RAF was estimated from this behaviour.

We use the method developed by some of us in Ref. [20] to estimate the mass portions of both amorphous phases, the MAF (mass fraction R), and the RAF (mass fraction $1-R$). We estimate R from the relation

$$R = \frac{[\langle v_h(T) \rangle - \langle v_h(T_g) \rangle]}{[\langle v_h(T) \rangle^{max} - \langle v_h(T_g) \rangle^{max}]} \quad (10)$$

where $\langle v_h(T_g) \rangle$ and $\langle v_h(T) \rangle$ are the hole volumes of the given polymer at T_g and at $T = T_g + 100$ K. $\langle v_h(T) \rangle^{max}$ and $\langle v_h(T_g) \rangle^{max}$ denote the corresponding values for $R = 100$. Assuming that the data for PFE correspond to $R = 100$, we estimate the following values for R: 0.52 (TFs), 0.52 (TFMs), 0.48 (PFAs), 0.22 (TFv), and 0.33 (TFMv).

The volumetric glass transition temperature of the PTFE samples with lower crystallinity corresponds well to the γ- (glass II) transition known from dynamic mechanical loss tests [39] and dielectric dilatometry [70]. In mechanical relaxation experiments the lowest tan δ peak (γ) occurs in melt-crystallised PTFE at −84 °C. This peak is replaced by a smaller loss peak at −66 °C in the virgin sample [39]. We remark that we have not detected a transition which could be attributed to the α- (glass I) transition observed in relaxation experiments at about 130 °C [39,70,71].

In Fig. 16 we show, as example, the number-weighted hole volume distribution $g_n(v_h)$ for TFMv and TFMs at low (−158 °C) and high (+200 °C) temperatures. The curves show, in agreement with Fig. 14, that at −158 °C the mean volume and its dispersion is smaller in TFMs than in TFMv. For higher temperatures these relation reverses: TFMs has the larger mean hole volume and dispersion.

3.4. The hole density

PALS itself is able to measure the mean volume of the holes and their size distribution, but not directly the hole density and the hole fraction. However, a correlation of PALS results either directly with the macroscopic volume V_a of an amorphous polymer or with its (excess) free volume V_f allows to estimate the hole density [26–32]. The mean

Table 2
Free volume parameters estimated from PALS data (see text)

Sample		TFv	TFs	TFMv	TFMs	PFAs	PFE
T_g (PALS, °C)	±5	−30	−80	−20	−83	−73	−8
$\langle v_{hg}\rangle$ (Å^3)	±7	166	147	140	152	138	166
α_{hr} (10^{-3} K^{-1})	±1.5	6.5	8.2	4.5	8.5	8.9	17.8
α_{hg} (10^{-3} K^{-1})	±0.5	0.7	0.8	∼0	2.1	0.20	2.2
N'_h (from V_f) (10^{21} g^{-1})	±0.01				0.127		0.161
N'_h (from V) (10^{21} g^{-1})	±0.01				0.123		0.157
$N_{hg} = N'_h/V_g$ (nm^{-3})	±0.02				0.27		0.32

number of holes per mass unit, N'_h, may be determined from one of the relations [26,31],

$$V_f = V_{f0} + N'_h\langle v_h\rangle \quad (11)$$

$$V_a = V_{occ} + V_{f0} + N'_h\langle v_h\rangle \quad (12)$$

In these equations, the specific free volume V_f is expressed by $N'_h\langle v_h\rangle$, the term V_{f0} may count for a possible deviation of the mean hole volume estimated from the *o*-Ps lifetime data from the true mean hole volume. Eqs. (11) and (12) are applied in past for amorphous polymers [26–32]. We attempt to use this method for our semicrystalline polymers and assume that here V_a is the specific volume of the entire amorphous phase, calculated from Eq. (1), and V_f is the corresponding excess free volume calculated from Eq. (5). $\langle v_h\rangle$ and N'_h are the mean volume and specific density of holes averaged over the entire amorphous phase.

Fig. 17 shows plots of V_f and V_a vs. $\langle v_h\rangle$ for TFMs. The data were taken from the temperature range between T_g+ 20 K (V_f and V_a extrapolated, see Figs. 5 and 6) and 40 °C where $\langle v_h\rangle$ varies linearly. One observes that both volumes, V_f and V_a, follow linear functions of $\langle v_h\rangle$. This behaviour is generally observed for amorphous polymers and from this it is concluded that N'_h is not a function of the temperature. For TFMs, the V_f vs. $\langle v_h\rangle$ plot leads to $N'_h = dV_f/d\langle v_h\rangle = 0.127(\pm0.01)\times10^{21}$ g^{-1} and a V_{f0} value being almost zero, $V_{f0} = 0.0044(\pm0.002)$ cm^3/g.

The V_a vs. $\langle v_h\rangle$ plot shows a slope of $dV_a/d\langle v_h\rangle = 0.137(\pm0.007)\times10^{21}$ g^{-1}.To estimate N'_h, this slope must be corrected for the expansion of the occupied volume, $N'_h = dV_a/d\langle v_h\rangle - dV_{occ}/d\langle v_h\rangle$. From the thermal expansion of V_{occ} and $\langle v_h\rangle$ we estimate $dV_{occ}/d\langle v_h\rangle = (dV_{occ}/dT)/(d\langle v_h\rangle/dT) = 1.8\times10^{-5}$ cm^3 g^{-1} K^{-1}/1.3 Å^3 K^{-1} = 0.014×10^{21} g^{-1} which leads to $N'_h = 0.123(\pm0.01)\times10^{21}$g^{-1} in agreement with the value estimated from V_f. The zero volume, $V_a(\langle v_h\rangle \to 0) = 0.444(\pm0.002)$ cm^3/g, correspond to $V_{occ}+V_{f0}$ (Eq. (11)). With $V_{f0} = 0.0044$ cm^3/g from the V_f vs. $\langle v_h\rangle$ plot we obtain $V_{occ} = 0.439(\pm0.003)$ cm^3/g which is in excellent agreement with the extrapolation of the occupied volume to 0 K, $V_{occ}(T\to0) = 0.442(\pm0.001)$ cm^3/g. The average of both N'_h values, $N'_h = 0.125(\pm0.01)\times10^{21}$g^{-1} correspond to a volume related hole number density of $N_h = N'_h/V_a = 0.27(\pm0.02)$nm^{-3} ($V_a = 0.4643$ cm^3/g at room temperature).

At this point we remark that we have concluded in a previous paper [32a] for PFE that the mean hole volume $\langle v_h\rangle^*$ of the corrected distribution $g_n(v_h)^* = g_n(v_h)/v_h$ follows better the specific free volume V_f (i.e. $V_f = 0$) than $\langle v_h\rangle$ does. From this we have concluded that *o*-Ps may prefer larger holes with a weight approximately proportional to the hole volume. This conclusion is not in disagreement with the results of this paper. Since the scatter in τ_4 and σ_4 are amplified in the calculation of $\langle v_h\rangle^*$ we have, however, not shown here the results of such analysis. Generally, $\langle v_h\rangle^*$ is somewhat smaller than $\langle v_h\rangle$, which leads to a larger value for the hole density when being estimated from $N'_h = V_f/\langle v_h\rangle^*$.

In Fig. 6 we have compared the specific free volume of

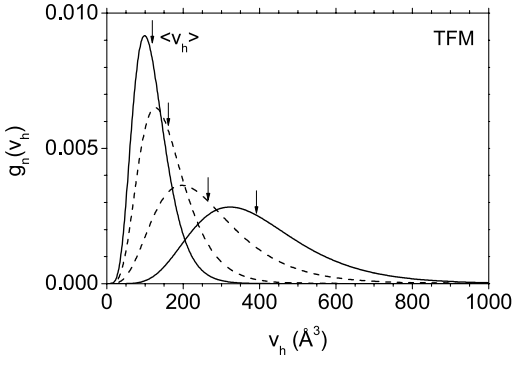

Fig. 16. Number-density hole volume distribution $g_n(v_h)$ normalized to $\int v_h g_n(v_h) dv_h = 1$ for TFM. Dashed line: virgin sample (TFMv), solid line: sintered, melt crystallized sample (TFMs); lower curves: −158 °C, upper curves: +200 °C. The arrows show the mean hole volume $\langle v_h\rangle$ of the distribution.

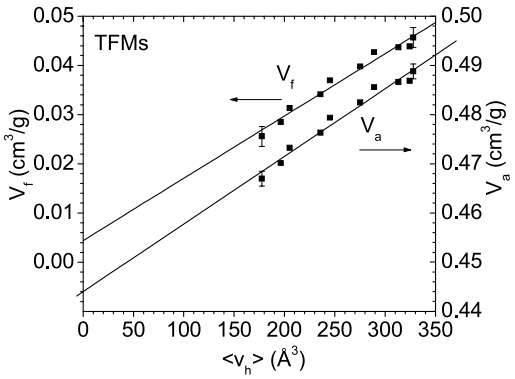

Fig. 17. Specific free volume V_f and specific total amorphous volume V_a plotted vs. the mean hole volume $\langle v_h\rangle$ (squares) for TFMs. The lines show linear fits to the data from the temperature range between −70 and +40 °C.

TFMs and TFMv directly, calculated from the relation $V_f = N'_h\langle v_h\rangle$ with N'_h as fitting parameter, with the specific free volume V_f estimated from the PVT experiments. For TFMs a good fit is obtained when assuming $N'_h = 0.143 \times 10^{21}$ g^{-1}, a value which is also obtained from the fit of the V_f vs. $\langle v_h\rangle$ plot constrained to pass zero, $V_{f0} = 0$. In case of the virgin sample we have calculated the value of V_f from the boundaries $V_{f,MAF}$ and $V_{f,RAF}$ assuming that the amorphous phase of this highly crystalline material consists of 0.75 parts as RAF and to 0.25 parts as MAF. A good agreement between this value for V_f and that calculated from $V_f = N'_h\langle v_h\rangle$ ($\langle v_h\rangle$ from TFMv) is obtained assuming a constant hole density of $N'_h = 0.26 \times 10^{21}$ g^{-1} (Fig. 6, lower part). One may conclude from this value that the RAF contains more holes than the MAF. The accuracy of the estimation is not very high and is based on several assumptions. A larger mean size and density of holes in the RAF below room temperature, compared with the MAF, however, correlates well with the higher specific volume (Fig. 5). Due to the inhibited expansion of holes in the RAF, the specific free and total volumes are above room temperature in the RAF lower than in the MAF.

4. Conclusions

(1) The specific volume of the MAF and RAF, V_{MAF} and V_{RAF}, of a semicrystalline polymer can be estimated when assuming that V_{MAF} agrees with the specific volume of the melt extrapolated down to lower temperatures using the S–S eos. V_{RAF} may then be estimated from the specific volume of the entire amorphous phase, V_a, assuming the mass ratio between RAF and MAF. V_a is estimated from the volume of the semicrystalline polymer using the known crystallinity and the know specific crystalline volume. Our estimations show that between room temperature and the melting point V_{RAF} is smaller than V_{MAF}. Below room temperature, the situation in PTFE reverses and at T_g the volume V_{RAF} is clearly larger than V_{MAF}. These relations are also valid for the specific free volume.

(2) The positron lifetime spectra show four components, the larger two are attributed to *o*-Ps annihilation in the interstitial free volume of crystals ($\tau_3 = 1.0$–1.15 ns) and in holes of the excess free volume in the amorphous phase ($\tau_4 = 1.5$–5 ns). The intensity of the third component, I_3, shows an increase around 20 °C attributed to the solid–solid transition of PTFE crystals. A clear change of τ_3 could not be observed, however, at this temperature. The number-weighted mean volume, $\langle v_h\rangle$, and the width, σ_h, of the hole size distribution, calculated from the parameters τ_4 and σ_4 of the LT9.0 analysis of lifetime spectra, show for the lowly crystalline, sintered, samples a typical glass transition behaviour: an abrupt increase in the coefficient of thermal expansion at T_g. T_g is estimated to be −80 °C for TFs and −83 °C for TFMs, −73 °C for PFAs, and −8 °C for the amorphous fluoroelastomer PFE. The mean hole density is found to be independent on the temperature and estimated from a comparison of V_f or V_a with $\langle v_h\rangle$ to be, for TFMs as example, $N'_h = 0.125(\pm 0.01) \times 10^{21}$ g^{-1} and $N_h = 0.27(\pm 0.02)$ nm^{-3}, respectively.

(3) The hole size of the virgin, highly crystalline PTFE shows even a glass transition, but with a higher T_g of −15 to −30 °C, and a smaller mean hole volume and expansivity above T_g. From this behaviour the ratio of RAF/MAF has been estimated to be 3 for the virgin polymers, and to be 1 for the melt crystallized samples. Apparently, some fraction of the amorphous phase occurs in a mobile state but with inhibited mobility. The mean hole volume, $\langle v_h\rangle$, and the width of the size distribution, σ_h, are below T_g larger than for the samples of low crystallinity. The hole density, N'_h, is larger than for the samples of low crystallinity. The behaviour of $\langle v_h\rangle$ and N'_h correlates well with the variation of specific volumes V_a and V_f analysed from the PVT experiments.

(4) The behaviour of the volume parameters $\langle v_h\rangle$, σ_h, N'_h, V_a, and V_f can be understood assuming that during crystallisation from the melt a fraction of the amorphous phase, the RAF, becomes restricted in its segmental mobility due to the incorporation of polymer chains into the crystals. This process is obviously associated with a denser molecular packing and a distinct loss of free volume compared with the unconstrained amorphous phase which shows, due to its high segmental mobility and the high temperature, strong thermal volume fluctuations and in the mean a larger specific free and total volume.

When lowering the temperature the contraction of the RAF slows down and finally, below room temperature in the current case, the RAF possess a larger hole volume and a larger specific free and total volume than the MAF shows. This behaviour mirrors the restriction of the segmental mobility in the RAF by the crystals which now inhibits further dense packing of the polymer chains. This denser packing occurs, however, in the MAF until T_g is reached.

Acknowledgements

We thank L. Häuβler and K. Arnold/Dresden for the DSC analysis and D. Kilburn/Bristol for his critical comments to the manuscript.

References

[1] Suzuki H, Grebovicz J, Wunderlich B. Br Polym J 1985;17:1.
[2] Wunderlich B. Prog Polym Sci 2003;28:383.

[3] Kitamaru R. Advances in polymer science. vol. 137. Berlin: Springer-Verlag; 1998. p. 42.
[4] Strobl G. Eur Phys J, E 2000;3:165.
[5] Schick C, Dobertin J, Pötter M, Dehne H, Hensel A, Wurm A, et al. J Therm Anal 1997;49:499.
[6] Schick C, Wurm A, Mohamed A. Colloid Polym Sci 2001;279:800.
[7] Alsleben M, Schick C. Thermochim Acta 2000;238:294.
[8] Tao SJ. J Chem Phys 1972;56:5499.
[9] Eldrup M, Lightbody D, Sherwood JN. Chem Phys 1981;63:51.
[10] Nakahishi N, Jean YC. Positron and positronium chemistry. In: Schrader DM, Jean YC, editors. Studies in physical and theoretical chemistry, vol. 57. Amsterdam: Elsevier Science Publication; 1988. p. 159.
[11] Pethrick RA. Prog Polym Sci 1997;22:1.
[12] Mogensen OE. Positron annihilation in chemistry. Berlin: Springer-Verlag; 1995.
[13] Jean YC, Mallon PE, Schrader DM, editors. Principles and application of positron and positronium chemistry. Singapore: World Scientific; 2003.
[14] Baugher AH, Kossler WJ, Petzinger KG. Macromolecules 1996;29: 7280.
[15] (a) Kindl P, Puff W, Sormann H. Phys Status Solidi A 1980;58:489.
(b) Kindl P, Sormann H, Puff W. In: Coleman PG, Sharma SC, Diana LM, editors. Positron annihilation. Proceedings of the sixth international conference. Amsterdam: North-Holland; 1982. p. 685.
[16] Wang CL, Wang B, Li SQ, Wang SJ. J Phys: Condens Matter 1993;5: 7515.
[17] Madani MM, Macqeen RC, Granata RD. J Polym Sci, Part B: Polym Phys 1996;34:2770.
[18] Dlubek G, Saarinen K, Fretwell HM. J Polym Sci, B: Polym Phys 1998;36:1513.
[19] Dlubek G, Stejny J, Lüpke T, Bamford D, Petters K, Hübner Ch, et al. J Polym Sci, B: Polym Phys 2002;40:65.
[20] Kilburn D, Bamford D, Lüpke T, Dlubek G, Menke TJ, Alam MA. Polymer 2002;43:6973.
[21] Olson BG, Lin J, Nazarenko S, Jamieson AM. Macromolecules 2003; 36:7618.
[22] Lin J, Shenogin S, Nazarenko S. Polymer 2002;43:4733.
[23] Zoller P, Walsh CJ. Standard pressure–volume–temperature data for polymers. Lancaster, Basel: Technomic Publications Co, Inc; 1995.
[24] Simha R, Somcynsky T. Macromolecules 1969;2:342.
[25] Utracki LA, Simha R. Macromol Theory Simul 2001;10:17.
[26] Dlubek G, Stejny J, Alam MA. Macromolecules 1998;31:4574.
[27] Srithawatpong R, Peng ZL, Olson BG, Jamieson AM, Simha R, McGervey JD, et al. J Polym Sci, Part B: Polym Phys 1999;37:2754.
[28] Schmidt M, Maurer FHJ. Polymer 2000;41:8419.
[29] Dlubek G, Bondarenko V, Pionteck J, Supey M, Wutzler A, Krause-Rehberg R. Polymer 2003;44:1921.
[30] Dlubek G, Pionteck J, Kilburn D. Macromol Chem Phys 2004;205: 500.
[31] Dlubek G, Bondarenko V, Al-Qaradawi IY, Kilburn D, Krause-Rehberg R. Macromol Chem Phys 2004;205:512.
[32] (a) Dlubek G, Sen Gupta A, Pionteck J, Krause-Rehberg R, Kaspar H, Lochhaas KH. Macromolecules 2004;37:6606.
(b) Dlubek G, Wawryszczuk J, Pionteck J, Goworek T, Kaspar H, Lochhaas KH. Macromolecules 2005;38:429.
[33] Hougham G, Cassidy PE, Johns K, Davidson T, editors. Fluoropolymers 2: properties. New York: Kluwer Academic/Plenum Publishers; 1996.
[34] Brandt W, Spirn I. Phys Rev 1966;142:231.
[35] Gregory RB. Nucl Instrum Methods Phys Res A 1991;302:496.
[36] Kansy J. Nucl Instrum Methods Phys Res A 1996;374:235.
[37] Kansy J. LT for Windows, Version 9.0, Inst of Phys Chem of Metals, Silesian University, Bankowa 12, PL-40-007 Katowice, Poland; 2002, private communication.
[38] Dlubek G, Supej M, Bondarenko V, Pionteck J, Pompe G, Krause-Rehberg R, et al. J Polym Sci, Part B: Polym Phys 2003;41:3077.
[39] Starkweather Jr HW, Zoller P, Jones GA, Vega AJ. J Polym Sci, Polym Phys Ed 1982;20:751.
[40] Starkweather HW. J Polym Sci, Polym Phys Ed 1982;20:2159.
[41] Starkweather Jr HW, Zoller P, Jones GA. J Polym Sci, Polym Phys Ed 1984;22:1431.
[42] Lau SF, Suzuki H, Wunderlich B. J Polym Sci, Polym Phys Ed 1982; 22:379.
[43] Rodgers PA. J Appl Polym Sci 1993;48:1061.
[44] Cohen MH, Turnbull D. J Chem Phys 1959;31:1164.
[45] Turnbull D, Cohen MH. J Chem Phys 1970;52:3038.
[46] Simha R, Wilson PS. Macromolecules 1973;6:908.
[47] Williams ML, Landel RF, Ferry JD. J Am Chem Soc 1955;77:3701.
[48] Dlubek G, Saarinen K, Fretwell HM. Nucl Instrum Methods Phys Res B 1998;142:139.
[49] Gregory RB. J Appl Phys 1991;70:4665.
[50] Liu J, Deng Q, Jean YC. Macromolecules 1993;26:7149.
[51] (a) Dlubek G, Eichler S, Hübner C, Nagel C. Nucl Instrum Methods Phys Res B 1999;149:501.
(b) Dlubek G, Eichler S, Hübner C, Nagel C. Phys Status Solidi A 1999;174:313.
[52] Dlubek G, Hübner C, Eichler S. Phys Status Solidi A 1999;172:303.
[53] Gregory RB, Zhu Y. Nucl Instrum Methods A 1990;290:172.
[54] (a) Shukla A, Peter M, Hoffmann L. Nucl Instrum Methods A 1993; 335:310.
(b) Hoffmann L, Shukla A, Peter M, Barbiellini B, Manuel AA. Nucl Instrum Methods A 1993;335:276.
[55] Bertolaccini M, Bisi A, Gambarini G, Zappa L. J Phys C 1974;7:3827.
[56] Lightbody D, Sherwood JN, Eldrup M. Chem Phys 1985;94:475.
[57] Kimming M, Strobl G, Stühn B. Macomolecules 1994;27:2481.
[58] Androsch R. J Polym Sci, Part B: Polym Phys 2001;39:750.
[59] Ito Y. Mater Sci Forum 1995;175-178:627.
[60] Nakanishi H, Jean YC. Macromolecules 1991;24:6618.
[61] Olson BG, Prodpran T, Jamieson AM, Nazarenko S. Polymer 2002; 43:6775.
[62] Xie L, Gidley D, Hristov H, Yee A. Polymer 1994;35:14.
[63] Wang DL, Hirade T, Maurer FHJ, Eldrup M, Petersen NJ. J Chem Phys 1998;108:4656.
[64] Hirade T, Maurer FHJ, Eldrup M. Radiat Phys Chem 2000;58:465.
[65] Roberson RE. In: Bicerano J, editor. Computational modeling of polymers. Midland, MI: Marcel Dekker; 1992. p. 297.
[66] Bueche F. J Appl Phys 1955;26738.
[67] Bamford D, Reiche A, Dlubek G, Alloin F, Sanchez JY, Alam MA. J Chem Phys 2003;1189420.
[68] Winberg P, Eldrup M, Maurer FHJ. Polymer 2004;45:8253.
[69] Hartmann L, Kremer F, Pouret P, Léger L. Molecular Dynamics in grafted layers of poly(dimethyl siloxane) (PDMS), arXiv:cond-mat/0208087v1 5Aug 2002.
[70] Schwödiauer R, Heitz J, Arenholz E, Bauer-Gogonea S, Baure S. J Polym Sci, Part B: Polym Phys 1999;37:2115.
[71] Rae PJ, Dattelbaum DM. Polymer 2004;45:7615.